

LA-UR-20-29392 (Accepted Manuscript)

Mechanistic modelling of SARS-CoV-2 and other infectious diseases and the effects of therapeutics

Perelson, Alan S.
Ke, Ruian

Provided by the author(s) and the Los Alamos National Laboratory (2021-01-25).

To be published in: Clinical Pharmacology & Therapeutics

DOI to publisher's version: 10.1002/cpt.2160

Permalink to record: <http://permalink.lanl.gov/object/view?what=info:lanl-repo/lareport/LA-UR-20-29392>

Disclaimer:

Los Alamos National Laboratory, an affirmative action/equal opportunity employer, is operated by Triad National Security, LLC for the National Nuclear Security Administration of U.S. Department of Energy under contract 89233218CNA000001. By approving this article, the publisher recognizes that the U.S. Government retains nonexclusive, royalty-free license to publish or reproduce the published form of this contribution, or to allow others to do so, for U.S. Government purposes. Los Alamos National Laboratory requests that the publisher identify this article as work performed under the auspices of the U.S. Department of Energy. Los Alamos National Laboratory strongly supports academic freedom and a researcher's right to publish; as an institution, however, the Laboratory does not endorse the viewpoint of a publication or guarantee its technical correctness.

Article type : State of the Art

Mechanistic modelling of SARS-CoV-2 and other infectious diseases and the effects of therapeutics

Alan S. Perelson^{1,2*} and Ruian Ke^{1,2}

¹ Theoretical Biology and Biophysics Group, Los Alamos National Laboratory, Los Alamos, NM 87545 USA

² New Mexico Consortium, Suite 301, Research Park, 4200 West Jemez Rd, Los Alamos, NM 87544 USA

*Corresponding author, email: asp@lanl.gov, telephone: +1-505-667-6829

Conflict of interest: The authors declared no competing interests for this work.

This article has been accepted for publication and undergone full peer review but has not been through the copyediting, typesetting, pagination and proofreading process, which may lead to differences between this version and the [Version of Record](#). Please cite this article as [doi: 10.1002/cpt.2160](https://doi.org/10.1002/cpt.2160)

This article is protected by copyright. All rights reserved

Funding: Portions of this work were done under the auspices of the US Department of Energy under contract 89233218CNA000001 and supported by NIH grants R01-OD011095, R01-AI028433 (ASP), and R01-AI15270301 (RK); and DARPA grant HR0011047746 (RK), as well as the US National Science Foundation RAPID grant PHY-2031756 (ASP).

Key words: Viral dynamics, viral kinetics, SARS-CoV-2, COVID-19, HIV, hepatitis C virus, influenza

Abstract

Modern viral kinetic modeling and its application to therapeutics is a field that attracted the attention of the medical, pharmaceutical and modeling communities during the early days of the AIDS epidemic. Its successes lead to applications of modeling methods not only to HIV but a plethora of other viruses, such as hepatitis C virus (HCV), hepatitis B virus (HBV) and cytomegalovirus (CMV), which along with HIV cause chronic diseases, and viruses such as influenza, respiratory syncytial virus (RSV), West Nile virus (WNV), Zika virus, and SARS-CoV-2, which generally cause acute infections. Here we first review the historical development of mathematical models to understand HIV and HCV infections and the effects of treatment by fitting the models to clinical data. We then focus on recent efforts and contributions of applying these models towards understanding SARS-CoV-2 infection and highlight outstanding questions where modeling can provide crucial insights and help to optimize non-pharmaceutical and pharmaceutical interventions of the COVID-19 pandemic. The review is written from our personal perspective emphasizing the power of simple target cell limited models that provided important insights and then their evolution into more complex models that captured more of the virology and immunology. To quote Albert Einstein “Everything should be made as simple as possible, but not simpler”, and this idea underlies the modeling we describe below.

Modeling HIV infection and treatment

Simple models^{1, 2, 3} of viral dynamics provided surprising insights into HIV infection. One critical element in modeling viral infections is keeping track of the change in viral load over time. For both HIV and HCV, which generate chronic infections, one usually finds that after the acute phase of infection, the virus and host come into accommodation, such that the viral load when measured over periods of days, weeks or months stays relatively constant. This constant level is called the viral set-point and to modelers, this means the viral-host system is at steady-state. To gain information about the underlying processes that generate and clear the virus, one can perturb the system from this steady state, for example by drug therapy. To understand the subsequent dynamics, what we now call the standard model of viral dynamics was introduced⁴. This model, as shown in Fig. 1, keeps track of

cells susceptible to viral infection, which virologists call target cells, T , infected cells, I , and virus, V and their dynamics are given by the following system of ordinary differential equations (ODEs):

$$\frac{dT}{dt} = s - d_T T - \beta VT \quad (1a)$$

$$\frac{dI}{dt} = \beta VT - \delta I \quad (1b)$$

$$\frac{dV}{dt} = pI - cV \quad (1c)$$

where target cells are generated at rate s , die at rate d_T per cell and become infected with rate constant β when virus, V , interacts with a target cell. Infected cells are generated at rate βVT and die at per capita rate δ . Lastly, virus, V , is produced by infected cells at rate p per cell and is cleared at rate c per virion. This system of equations (1) has been successfully used to model acute HIV infection if one assumes that initially all cells are uninfected and at time $t=0$ a small amount of virus is introduced into the body⁵. The model predicts that virus initially grows exponentially, reaches a peak, and then settles at a constant level, called the set-point (Fig. 2A).

The model has also been used to analyze the effects of antiretroviral therapy (ART) by incorporating into the model the effects of antiretroviral drugs. For example, reverse transcriptase (RT) inhibitors block the ability of HIV to productively infect a cell. HIV protease inhibitors (PI) cause infected cells to produce immature non-infectious viral particles, V_{NI} . Thus, in the presence of these drugs, the model equations become^{3, 6}

$$\begin{aligned} \frac{dT}{dt} &= s - d_T T - (1 - \epsilon_{RT})\beta V_I T \\ \frac{dI}{dt} &= (1 - \epsilon_{RT})\beta V_I T - \delta I \\ \frac{dV_I}{dt} &= (1 - \epsilon_{PI})pI - cV_I \\ \frac{dV_{NI}}{dt} &= \epsilon_{PI}pI - cV_{NI} \end{aligned} \quad (2)$$

where ε_{RT} and ε_{PI} taken on values between 0 and 1, and represent the efficacies of RT and PI inhibitors ($\varepsilon=1$ being a 100% effective drug). Further, V_I and V_{NI} are the concentrations of “infectious” and noninfectious virus, respectively, and $V=V_I+V_{NI}$ is the total virus concentration. An HIV entry inhibitor can be modeled in the same way as an RT inhibitor.

Equations (2) can be solved analytically if one assumes that during short-term therapy the number of target cells, T , remains at its baseline pre-therapy steady state value, $T_0=c\delta/\beta p$, and that therapy is with a 100% effective protease inhibitor ($\varepsilon_{PI}=1$, $\varepsilon_{RT}=0$). The solution is^{3,6}

$$V(t) = V_0 \exp(-ct) + \frac{cV_0}{c-\delta} \left(\frac{c}{c-\delta} [\exp(-\delta t) - \exp(-ct)] - \delta t \exp(-ct) \right), \quad (3)$$

where V_0 is the set-point viral load before initiation of therapy. This solution only depends on three parameters, V_0 , c and δ . Allowing the target cell concentration, T , to vary necessitates using numerical methods to predict $V(t)$ but does not substantially alter the outcome of the analysis.

Fitting either the analytical solution (3) or the numerical solution of $V(t)$ to patient derived viral decline data allowed the first estimates of the rate of viral clearance, c , and the death rate of infected cells, δ , in vivo to be obtained³. These estimates were minimal because in reality protease inhibitors are not 100% effective (see Ref. ³ for details). Later analysis using the same method but fitting to data obtained from patients treated with a four drug combination that is closer to being 100% effective yielded an estimate of $\delta = 1.0/\text{day}$ ⁷. This implies that productively infected cells have an average lifespan, $1/\delta$, of about 1 day while producing virus and decay with a half-life $t_{1/2} = \ln 2 / \delta = 0.7$ days. The first estimate of c was 3/day, which corresponds to a half-life of virus in the circulation of $t_{1/2} = 6$ hrs. This estimate was not very accurate because drug does not act instantaneously after administration and later work showed the half-life to be closer to 45 min, i.e., $c \sim 23/\text{day}$ ⁸. Further, because $c \gg \delta$ (i.e., 23/day vs 1/day) one would expect from Eq (3) that the terms involving $\exp(-ct)$ would rapidly decay leaving the dominant decay to be proportional to $\exp(-\delta t)$.

One very important finding from this model was an estimate of how much virus was produced daily throughout the entire body. At the pre-therapy steady state, the total body wide rate of production of virus must equal the total viral clearance rate. The term cV_0 gives the rate of clearance from 1 mL of

blood plasma before therapy starts. The total extracellular body water in a 70 kg adult is approximately 15 liters. Thus, for an individual with an initial viral load of 10^5 HIV RNA copies/ml and $c=23/\text{day}$, we can estimate that 3.5×10^{10} HIV RNAs are produced and cleared per day. This is a minimal estimate because some HIV is also in attached to cells in tissue. Because HIV mutates when it replicates one can compute that every possible single mutation and most double mutations are made every day^{9, 10}. This observation suggested that combinations of three drugs should be used to treat HIV infections. When such combination therapy was given to chronically infected HIV individuals, the virus was observed to decline in two exponential phases, a fast first-phase followed by a slower second-phase (Fig. 2B). The second phase was attributed to the existence of a population of “long-lived infected cells”, with the slope of the second phase reflecting the death rate of these cells¹¹.

One can analytically solve Eqs. (2) for any combination of protease inhibitor and reverse transcriptase inhibitor of any efficacy as long as one assumed that target cell level remained constant, as this made the system of equations (2) linear⁶. However, for HIV *in vivo*, drug efficacies were not known and analysis of the solutions to these linear equations showed that models still predicted exponential decays but now with eigenvalues that included the drug efficacy. Thus, simply fitting these models to data that exhibited exponential decays did not allow one to estimate the drug efficacy. Experiments done with combination therapy showed that the first-phase viral decay slope increased and when comparing different drug regimes, the ratio of such slopes was used as a measure of the relative efficacy of one regime versus another¹². Also, later elaborations of the basic model used to describe the effects of therapy for HIV and HCV (discussed below) replaced the constant drug efficacies in this simple model by models in which the drug efficacy was allowed to change in time to mimic pharmacokinetic (PK) effects¹³ or by using full PK/pharmacodynamic models^{14, 15, 16, 17, 18}.

After a cell is first infected by a virus it does not instantly start producing new progeny virions. Rather there is a period time called the eclipse phase during which no virus is produced by the cell. More biologically accurate models have been developed that include the eclipse phase. In the case of HIV this was first modeled by Herz et al.¹⁹ by a fixed time delay of length τ . Thus, in their model Eq. (1b) for productively infected cells was replaced by

$$\frac{dI}{dt} = \beta(t - \tau)V(t - \tau)T(t - \tau)e^{-m\tau} - \delta I, \quad (4)$$

where m is the mortality or death rate of a cell in the eclipse phase and the term $\exp(-mt)$ represents the fraction of initially infected cells that remain alive at time t . A more realistic model introduced by Mittler et al.²⁰ assumed a distributed delay and replaced Eq. (4) by

$$\frac{dI}{dt} = \int_0^t f(\tau)\beta(t-\tau)V(t-\tau)T(t-\tau)e^{-m\tau} d\tau - \delta I, \quad (5)$$

where $f(\tau)$ is the probability distribution for the delay. If $f(\tau)$ is chosen as a Dirac delta function then Eq. (5) reduces to Eq. (4), so Eq. (5) is a rather general formulation. They then went on to study the case in which the delay distribution was given by a gamma function with an integer shape parameter, i.e. an Erlang distribution. They also showed that Eq. (5) could be converted to a set of n ordinary differential equation, where n is the integer shape parameter of the gamma distribution, which is sometimes convenient when fitting the model to data. Using such a model to fit patient viral decline data leads to slightly changed estimates of the basic parameters c and δ ^{19, 21}. Similar analyses were done for influenza and also showed that the choice of the delay distribution affects parameter estimates²². For *in vivo* modeling, there is generally not frequent enough sampling to accurately predict the additional parameters introduced by this approach. However, it has been useful to more precisely fit models to data from *in vitro* HIV/SHIV infection experiments²³. In modeling other infections, such as influenza²⁴ and Zika^{25, 26}, cells in the eclipse phase were explicitly modeled as a separate population of infected cells. Thus, Eq. (1b) and (1c) were replaced by the equations

$$\frac{dI_1}{dt} = \beta VT - kI_1 \quad (6a)$$

$$\frac{dI_2}{dt} = kI_1 - \delta I_2 \quad (6b)$$

$$\frac{dV}{dt} = pI_2 - cV \quad (6c)$$

where I_1 represents cells in the eclipse phase and I_2 represents productively infected cells, i.e. cells that produce virus. For these acute infections, one advantage of including the eclipse phase is that the models then generated more realistic estimates for the lifespan of an infected cell as it now includes the time spent in the eclipse phase plus the time in the productive phase of infection, i.e. $1/k + 1/\delta$ ²⁴.

Another modeling approach that has been used to account for the delay between the time of infection and the start of viral production is to use an age-structured model where age, a , represents the time a cell has been infected. In this approach, Eqs. (1b) and (1c) of the basic model are replaced by

$$\frac{\partial I}{\partial a} + \frac{\partial I}{\partial t} = -\delta(a)I(a,t) \quad (7a)$$

$$\frac{dV}{dt} = \int_0^\infty p(a)I(a,t)da - cV, \quad (7b)$$

where the death rate of infected cells and the rate of viral production are now functions of how long a cell has been infected. Initially the viral production rate would be zero, i.e. $p(0)=0$ and then it could increase as a step-function, which would mimic having a fixed delay, or more realistically the viral production rate, after a delay, could increase gradually to a maximum level²⁷.

Before HIV modeling was done there was no quantitative information about how HIV acted *in vivo* and it was mistakenly thought that the kinetics must be slow because it took on average 10 years for AIDS to develop into a full-blown disease. Thus, the major impact of this work was to show that at set-point the virus was not turning over slowly, but rather there was rapid production and clearance of both virus and infected cells. This led to the introduction of combination therapy and the hope that with potent enough drugs HIV could be cured. However, this was not to be. A population of latently infected cells that harbor the HIV genome, but which do not produce virus unless activated, were found to decay under potent therapy with a half-life of 44 months²⁸. Based on estimates of the number of these cells in the body, it was calculated that it would take about 60 years of completely effective therapy to eliminate HIV²⁸. Current efforts are being made to accelerate the elimination of the latent reservoir using pharmacological and immunological methods²⁹.

Modeling HCV infection and treatment

HCV is a positive strand RNA virus that primarily infects human hepatocytes and like HIV can lead to chronic infection. About 180 million people are infected world-wide and there is no vaccine for it yet. The standard therapy for HCV for over a decade had been a combination of interferon- α (IFN), or

pegylated interferon- α (PEG-IFN), and the nucleoside analog ribavirin (RBV). When given for 48 weeks, this combination was able to cure slightly less than 50% of patients with HCV genotype 1 infection, the most common form of infection in the US and Europe. In May 2011, the first direct acting antiviral (DAA) for the treatment of HCV, the HCV protease inhibitor telaprevir, was approved. Subsequently, many other DAAs have been approved. Unlike HIV, HCV does not have a DNA form and its RNA genome replicates in the cytoplasm of a cell. The replication can be stopped by drug therapy, and the HCV RNA within a cell can degrade. Probably because of this biology, combination therapy with two or three DAAs with different mechanisms of action has led to cure in almost all treated individuals.

Mathematical modeling played an important role in characterizing HCV kinetics, determining basic quantities such as the lifespan of infected cells and the clearance rate of HCV from the circulation as well as providing insight into the mechanism of action of DAAs. Work in this area began with the basic model, Eqs. (1a)-(1c), which when used to analyze the plasma viral declines in patients treated with IFN led to the realization that IFN acted to reduce the rate of viral production from infected cells, p . Interferon is a cytokine that binds IFN receptors and signals through these receptors, turning on hundreds of interferon-stimulated genes, whose gene products ultimately reduce viral production within an infected cell.

The viral declines were biphasic, like for HIV, but the first phase was considerably faster and only lasted 1-2 days and then was followed by a slower second phase decline (Fig. 3). Because IFN at doses of 10-15 MIU daily could reduce p by 95%, the first phase slope largely reflected the rate of viral clearance whereas the second phase slope largely reflected the rate of death of productively infected cells³⁰. The following simple mathematical analysis led to a way to rapidly evaluate the *in vivo* effectiveness of IFN and later DAAs used to treat HCV. For a drug that affects viral production, the basic model equation (1c), should be modified such that the viral equation becomes

$$\frac{dV}{dt} = (1 - \epsilon)pI - cV, \quad (8)$$

where $0 \leq \varepsilon \leq 1$ is the effectiveness of therapy in blocking viral production. Note that, at the pre-therapy set-point, $pI_0 = cV_0$, where the subscript 0 denotes the baseline value before therapy. If one assumes that over the first day of therapy the number of infected cells stays at I_0 , then Equation (7), with the initial condition $V(0) = V_0$, can be solved to yield

$$V = V_0, \text{ for } t < t_0$$

$$V(t) = V_0[1 - \varepsilon + \varepsilon e^{-c(t-t_0)}], \quad \text{for } t \geq t_0, \quad (9)$$

where t_0 is the pharmacological delay before IFN becomes effective. As c turns out to be about as large for HCV as for HIV³¹, V rapidly approaches $V_0(1-\varepsilon)$. Note that this implies that, if a drug is 90% effective, i.e. if $\varepsilon=0.9$, then the viral load will rapidly decline by one log, whereas if it is 99% effective the decline will be two logs. Thus, from the magnitude of the first phase viral load decline one can get an estimate of the effectiveness of an HCV antiviral agent. This led to the estimation that the active tissue concentration of the HCV NS5A inhibitor, daclatasvir, is much lower than its plasma concentrations³². Moreover, this estimate can be made in a one- or two-day clinical trial. For this reason, the first HCV protease inhibitor to go into human trials, BILN-2061, was given for only two days³³ and, using a viral kinetic model, the effectiveness, ε , was estimated to be above 99.5% in patients with mild disease³⁴.

As the first phase is over after one or two days, data collected over the subsequent week or two allowed one to estimate the death rate of productively infected cells, δ . For IFN therapy, on average $\delta = 0.14/\text{day}$ ^{30, 35}. The same methodology was used to analyze the effects of DAA therapy. Interestingly, although two-phase viral declines were always seen, the estimates of c and δ varied with the drug under study. As these parameters should depend on the host's ability to clear virus and infected cells, the application of the basic model was called into question and a multiscale model that tracked intracellular steps in the viral life cycle was developed. In particular, an equation was added to the basic model that followed the amount of intracellular positive strand HCV RNA, R , that was in a cell infected for time a . This generated the following age-structured model:

$$\frac{dT}{dt} = s - dT - \beta VT$$

$$\frac{\partial I}{\partial a} + \frac{\partial I}{\partial t} = -\delta I(a,t)$$

$$\frac{dV}{dt} = (1 - \varepsilon_s)\rho \int_0^{\infty} R(a,t)I(a,t)da - cV \quad (10)$$

$$\frac{\partial R}{\partial a} + \frac{\partial R}{\partial t} = (1 - \varepsilon_\alpha)\alpha - \kappa\mu R - (1 - \varepsilon_s)\rho R$$

with boundary conditions $I(0,t)=\beta VT$, $I(a,0)=I_0(a)$, $R(0,t)=1$, $R(a,0)=R_0(a)$, where $I_0(a)$ and $R_0(a)$ are the pre-therapy steady state distributions and α is the rate of viral RNA (vRNA) synthesis, μ is the rate of vRNA degradation and ρ is the rate of vRNA loss due to incorporation into secreted virions. It was assumed that treatment begins at time $t=0$ and that cells when initially infected contain one vRNA. The treatment effects of an antiviral drug were assumed to be blocking vRNA synthesis with effectiveness ε_α , blocking viral assembly/secretion with effectiveness ε_s and increasing the rate of vRNA degradation by the factor κ . By integrating over the age-structure, Kitagawa et al.³⁶ showed that these equations could be converted into a system of ordinary differential equations. Fitting this model to data from therapy with the HCV NS5A inhibitor daclatasvir and to data with the HCV protease inhibitor telaprevir, Guedj et al.³¹ predicted that both of these drugs had two modes of action, blocking vRNA synthesis and blocking viral assembly secretion, with efficacies of 99% or greater for daclatasvir. These predicted modes of action were then verified by *in vitro* experiments^{31, 37, 38}. Multiscale model of hepatitis B virus (HBV) infection and treatment are now also being developed³⁹ and should prove useful in analyzing the effects of new classes of HBV therapeutics currently in clinical development.

Modeling SARS-CoV-2 infection and treatment

Viral dynamic models for chronic infections above can be adapted to quantify dynamics of acute infections, such as influenza^{24, 40}, West Nile virus⁴¹, RSV⁴², Zika²⁶ and SARS-CoV-2^{43, 44, 45, 46, 47, 48, 49, 50, 51, 52, 53}. In particular, extensive modeling efforts have been made towards understanding influenza infection and the immune response against it. These studies often serve as the basis for modeling

other acute infections. See Refs. ^{54, 55} for recent reviews of within-host influenza models. Because of the current interest in COVID-19, below we will focus on the models for SARS-CoV-2 infection, summarize key recent findings from these models and highlight outstanding questions relevant for non-pharmaceutical interventions as well as the development of therapeutics and vaccines.

SARS-CoV-2 is a single-stranded RNA virus that causes acute infection of the respiratory system. Viral loads are often measured in hospitalized patients (see Fig. 4 for a schematic) to understand the course of infection and clinical outcomes^{56, 57}, and in non-human primate (NHP) infections to evaluate the efficacy of therapeutics, e.g. the antiviral remdesivir⁵⁸. With the availability of clinical and experimental data, many mathematical models have been developed and calibrated with data^{43, 44, 45, 46, 47, 48, 49, 50, 51, 52, 53}. Overall, these studies greatly advanced our quantitative understanding of SARS-CoV-2 infection in both humans and NHPs, the immune responses and the impact of therapeutics.

Target cell limited model

The simplest form of acute infection model, that is often used as a starting point to understand SARS-CoV-2 infection dynamics in many studies^{43, 44, 47, 51}, is derived from the basic viral dynamic model given by Eqs. (1). This model incorporates target cell replenishment and therefore allows the viral load to reach a steady state in which virus and infected cell production balances their clearance. In order to model acute infections where natural death and replenishment of target cells are negligible during the short period of infection, Eq. (1a) can be simplified to

$$\frac{dT}{dt} = -\beta VT. \quad (11)$$

This model is termed the target cell limited model, because the dynamics of this model are driven by the availability of target cells. During early infection, target cells are abundant, and thus the virus population grows exponentially until a viral peak is reached and most target cells are infected. Then, the viral load declines exponentially towards extinction because there are few target cells left in the system. The dynamics of the model are very similar to the often-used Susceptible-Infected-Recovered

(SIR) model in epidemiology where epidemics spread through a population until the population runs out of susceptible individuals.

A simplification that one can make is to assume the time scales of virus production and clearance are much quicker than the dynamics of infected cells, and thus the dynamics of viruses are in quasi-equilibrium with infected cells: $\frac{dV}{dt} \approx 0$, and thus $V = \frac{p}{c}I$. This assumption simplifies the 3-ODE system to a 2-ODE system. A variation of this simplification has been used compare infection dynamics of SARS-CoV-1, SARS-CoV-2 and MERS⁵⁰.

An extension of the basic model above is to add an eclipse phase for infected cells, because it usually takes hours for infected cells to start to produce viral particles. The simplest form of an eclipse phase model given by Eqs, (6a-6c) has been used in SARS-CoV-2 modeling. This allows for more accurate estimation of parameter values in the model as well as composite parameters of interest, such as the within-host reproductive number R_0 .

Estimating key parameter values

One key challenge in modeling a novel viral infection, such as SARS-CoV-2 infection, is that key parameter values such as the number of target cells in the model are unknown. Efforts have been made to estimate these parameter values from data^{44, 48, 49, 50}. For example, single cell gene expression data suggests that approximately 1% of cells in the respiratory tracts express the receptor and the coreceptor for SARS-CoV-2 entry, i.e., angiotensin-converting enzyme 2 (ACE2) and the type II transmembrane serine protease TMPRSS2^{59, 60}. Based on this finding, we estimated that there are approximately 4×10^6 and 4.8×10^8 target cells for SARS-CoV-2 in the URT and LRT respectively⁴⁹. This represents a rough estimate, because whether a cell is a target of infection may also depend on other factors in addition to gene expression⁶¹. Another parameter that can be calculated directly from experimental data is the duration of the eclipse period, $1/k$. *In vitro* experiments have shown that it usually takes 4-8 hours before an infected cell starts to produce SARS-CoV-2 particles^{61, 62}. It is not

known how quickly virus particles are cleared from the respiratory tract. Initial guesses of this parameter are based on estimates from influenza infection^{24, 40}.

Fitting the TCL model to viral load data, we and others have estimated that the death rate of infected cells ranges between 0.5 and 4 per day^{44, 48, 49, 50}. The value of R_0 is estimated to be between 5 and 30^{44, 49}. The parameter p usually cannot be identified but only the product pT_0 ⁵. In a SARS-CoV-2 model fit to data where T_0 was fixed and the viral load was measured per swab, only the product of p and the fraction of viruses sampled could be estimated⁴⁹.

Overall, there still exists considerable levels of variation in estimated parameter values across studies. This partially reflects heterogeneities in the viral dynamics among individual patients and in different physiological compartments. They also likely arise from uncertainties in the dataset itself as we will discuss in the Outstanding questions section.

Innate immune model

The innate immune response represents the first line of defense against viral infections and thus may impact on the dynamics of SARS-CoV-2 infection kinetics. One important arm of the innate immune response is the antiviral response triggered by type I interferon (IFN)⁶³. The production of IFN by infected cells and the subsequent autocrine and paracrine signaling can lead to an antiviral state in both infected cells and target cells. This in turn can lead to a reduction in virus production in infected cells and protection of target cells from infection. IFN also induces the recruitment of immune cells such as macrophages and natural killer cells to the site of infection⁶³. This recruitment may lead to increased killing of infected cells.

To model the protection of target cells by IFN signaling in influenza infection, Pawelek et al. added a refractory cell compartment⁴⁰. Similar formulations were used for SARS-CoV-2 infection^{44, 46, 49}. The ODEs for the target cell population (T), the refractory cell population (R) and interferon (F) from Eqs. (1) are then modified to

$$\begin{aligned}\frac{dT}{dt} &= -\beta VT - \phi FT + \rho R \\ \frac{dR}{dt} &= \phi FT - \rho R \\ \frac{dF}{dt} &= \pi I - wF\end{aligned}\tag{12}$$

where ϕ is the rate at which IFN causes a target cell to become refractory to infection, ρ is the rate at which the refractory state is lost, π is the rate of IFN production from an infected cell and w is the rate of IFN loss. Using this formulation, we recently found that adding the IFN response to the model does not significantly improve the fits to a set of data collected from 8 patients compared to the target cell limited model⁴⁹. This could indicate that the IFN response is inhibited and does not play an important role in reducing viral load in these patients, consistent with experimental studies showing that the IFN signaling pathway is suppressed during SARS-CoV-2 infection⁶⁴; or it is possible that the role of interferon cannot be statistically distinguished with this set of viral load data.

To model the recruitment of innate immune cells and thus increased killing of infected cells, Goyal et al.⁴⁵ used a term $-\delta I^n$ (instead of $-\delta I$) in the infected cell equation to model the dependence of infected cell killing on the innate response. This formulation was originally developed to model the immune dependent killing of infected cells during HIV infection⁶⁵, and also later used in influenza modeling⁶⁶. The underlying assumption is that the immune cell mediated killing is determined by the size of the immune cell population, which in turn is dependent on the infected cell population. Goyal et al. found that this model was able to describe the rapid decrease in viral load observed immediately after the initial viral peak (Fig. 4) and predicts that the viral load decline rate decreases as viral load declines to a low level⁴⁵.

Despite the majority of modeling work focusing on well-mixed models, an important aspect of acute respiratory infections is the spatial nature of the infection process in respiratory tract epithelium⁶⁷. As discussed above, well-mixed models in general predict that the IFN response affects peak viral load and viral dynamics afterwards^{24, 40}. In contrast, recent works of ours pointed out when target cells are spatially segregated, e.g., in epithelium, the combined impact of autocrine and paracrine signaling can strongly suppress viral spread during early infection before the viral peak^{68, 69}. These types of models may be important in understanding how early IFN response or treatment determines long-term infection outcome as suggested recently by experimental studies of SARS-CoV-2 and MERS coronavirus^{64, 70, 71}.

The quantitative impact of the IFN response on SARS-CoV-2 dynamics and which aspect of the response plays a more important role still need to be resolved. Also, the responses may vary from individual to individual. Simultaneously measuring the viral load and levels of interferon over time may help to resolve the question. In a study of Zika virus infection in nonhuman primates, IFN levels were measured along with viral load and including these IFN level in an immune response model did not improve the fit of the model to data over that using a target cell-limited model²⁵. However, Zika like many other viruses including HCV and SARS-CoV-2 antagonizes the IFN response. Including the effect of antagonism in a modified innate immune response model to Zika virus then improved the model fit over that of the target cell-limited model⁷². To further elucidate the phenomenon of antagonism, Padmanabham et al.⁷³ introduced a more detailed model of the intracellular IFN signaling network. They showed that HCV induces bistability in the network, causing the emergence of a new steady state where HCV persists⁷³. Whether this is also the case for SARS-CoV-2 remains to be determined

Adaptive immune model

Adaptive immune responses to SARS-CoV-2 infection develop one to two weeks after infection^{56, 74}. The most simplistic approach to model the impact of adaptive immune responses is to assume that the killing rate of infected cells increases after some time post-infection⁴⁰. This increase in infected cell killing rate may arise from the development of antigen-specific effector cells, such as cytotoxic T cell responses^{74, 75}. This approach involves adding only one or two extra parameters to an existing model, and thus is particularly well-suited for model calibration with data. Several studies have adopted this approach to understand SARS-CoV-2 infection dynamics beyond 2 weeks after infection^{45, 49, 51}. In general, the increased killing explains the rapid viral load decreases that accompany viral clearance (see the solid blue line in Fig. 4). A more complex model that keeps track of the maturation of precursor cells into immune effector cells has been proposed⁴⁵. This model effectively introduces a delay, as was done in modeling the eclipse phase with an Erlang distribution discussed earlier in the section on HIV infection models²⁰. However, the parameters governing the immune effector response need to be calibrated and validated with experimental/clinical data measuring the kinetics of the T cell response and the expansion of the relevant immune cell populations. Another important consideration for models explicitly including T cell populations is individual heterogeneity in initial T cell populations, because some individuals due to prior infection with seasonal coronaviruses may have some pre-existing cross-reactive T cell immunity to SARS-CoV-2⁷⁵. Simple models of both the CD4⁺ and CD8⁺ T cell response to lymphocytic choriomeningitis virus (LCMV) infection in mice have been developed and model parameters estimated⁷⁶. Also, a model of a dynamic motif underlying the interactions of antigens and CD8⁺ T cells was introduced in a rather general setting and then applied to LCMV and HCV infections⁷⁷. Models of this type should be tried for SARS-CoV-2 infection.

In contrast to the approaches above, where the models focused only on key aspects of the immune response and their impact on viral dynamics, another approach is to incorporate much more detailed information about the innate and adaptive immune responses as well as comorbidities induced by the virus. This is being done using multiscale simulation-based models^{78, 79, 80}. These models keep track of the complex molecular interactions involved in viral infection and virus replication within cells as well as spatial spread of the virus, the production of cytokines and chemokines, and the population

dynamics of various types of immune cells, such as macrophages, neutrophils, CD4⁺ T cells, CD8⁺ T cells, etc. This modeling approach offers a unique opportunity to integrate existing knowledge about viral infection and the induced response of various immune molecules and cells. However, one important challenge of this approach is validating the plethora of details included in these models against data to make reliable predictions, because of the large number of parameters in these models and the high levels of uncertainty about their values in the context of SARS-CoV-2 infection.

URT/LRT model

SARS-CoV-2 causes distinct infection dynamics in different tissue compartments⁵⁷ (Fig. 4). Infection in the upper respiratory tract (URT) exhibits typical acute infection dynamics⁵⁷. After an initial viral peak, the viral load decreases rapidly to low or undetectable levels. In contrast, sputum samples, likely representing dynamics in the lower respiratory tract (LRT), taken from hospitalized patients with mild disease⁵⁷, showed sustained intermediate-to-high viral loads for 3-4 weeks (Fig. 4). In some individuals, multiple viral load peaks were observed late in the infection. Motivated by these observations, we developed a two-compartment model to keep track of these distinct dynamics⁴⁹. Models including a URT and an LRT have also been used to understand viral dynamics in non-human primates where viral load measurements were taken from both nasal swabs and BAL^{46, 49, 53}. This type of model allows one to investigate the relationship between virus replication in different tissue compartments. For example, we have found that the rate of virus replication is positively correlated in the URT and the LRT⁴⁹ in the patients studied in Wolfel et al.⁵⁷. The rate of transport of virus from the URT to the LRT is probably low as mucocilliary clearance acts to bring particles out of the LRT. When virus does get into the LRT disease typically becomes more severe. Both the viral dynamics and some genetic sequencing information⁵⁷ suggest there may be compartmentalization of virus populations.

Viral spread in the LRT and cell proliferation

Viral loads in the lower respiratory tract (LRT) are positively associated with disease outcomes^{81, 82}. As mentioned above, viral loads in the LRT are maintained at intermediate-to-high levels for a prolonged period^{57, 82} (Fig. 4). Several mechanisms have been proposed to explain this pattern, including spatial spread of the virus and target cell proliferation^{46, 47, 49}. We recently explored these hypotheses, and showed that spatial spread into new areas of the lungs could explain sustained viral shedding as well as multiple viral load peaks⁴⁹. Type II alveolar cells, a major target cell population, proliferate in response to epithelial cell death and tissue damage⁸³. Cell proliferation can be modeled by adding the term $\rho T \left(1 - \frac{T+I}{T_0}\right)$ to Eqn. (1) for the target cell population, where T_0 is the total number of target cells in the absence of infection⁴⁹. This type of logistic term has been used for target cell proliferation in models of HIV, HCV and HBV infections^{84, 85, 86}. We found that a proliferation model of this type can explain the long-term persistence of viral load better than the target cell limited model or models incorporating the IFN response⁴⁹.

Overall, these model results suggest that new target cells for virus infection are needed to maintain the observed viral load. These can come from target cell proliferation or spatial spread of the virus to a new physiological compartment in the lungs. These insights may have important implications for therapeutic development to reduce disease severity. Other models were also proposed. For example, a model assumes that SARS-CoV-2 infects lymphocytes and predicts that the recruitment of lymphocytes to the infection site leads to sustained high viral loads⁵¹. However, the experimental evidence for lymphocytes being a major target for SARS-CoV-2 infection is not clear and the article cited in ref [51] as support for this hypothesis has been retracted.

Modeling therapy

As discussed earlier, mathematical models are widely used to estimate the efficacy of therapeutics in suppressing virus replication or infection^{1, 3, 4, 11, 24, 25, 30, 31}. Studies have used terms of the form $(1-\epsilon)$, where ϵ varies between 0 and 1 to represent the drug efficacy, to understand the impact of potential

therapeutics on SARS-CoV-2 infection dynamics^{43, 44, 45, 49, 50, 51}. A converging conclusion emerges that therapeutics that block virus replication and spread have to be administered before or at the time of peak viral load; otherwise, the therapeutics will not be effective at reducing overall host exposure to viruses⁴⁴ (Fig. 4). This is because most target cells are predicted to be infected by the time the peak viral load is reached and thus most viruses are produced during this period. Administration of therapeutics after peak viral load would only prevent a small fraction of total cell infections. For SARS-CoV-2, it has been estimated that peak viral load occurs at the time of or a couple of days after symptom onset^{44, 49, 87} and many infected individuals never show symptoms⁸⁸. Thus, it is most effective to administer antivirals or other therapeutics that block virus infection as soon as one tests positive or shows symptoms rather than later in the infection when severe symptoms develop (Fig. 4). This may partially explain the conflicting results from remdesivir trials where the antiviral was administered several days after symptom onset^{89, 90}. This also implies that we need antivirals that can be administered orally at home in addition to drugs such as remdesivir or the monoclonal antibodies now in clinical trials that need to be infused.

Drug efficacy can be modeled as a function of drug concentration by $\epsilon = \frac{C}{C + EC_{50}}$, where C represents drug concentration and EC_{50} is the concentration of the drug that gives half-maximal response. More detailed approaches to model PK/PD of SARS-CoV-2 antivirals were done for lopinavir/ritonavir, hydroxychloroquine, interferon- β -1a⁴⁴ and remdesivir and antibodies⁴⁵. However, parameter values in these PK/PD models are in general estimated from *in vitro* studies, non-human primates, or plasma of humans. A challenge is to estimate/validate parameter values at the relevant tissue compartments *in vivo*. As estimated previously for HCV antivirals, the active concentration at relevant tissue can be very different from that in plasma³². With appropriate data, this type of model framework can be used to design and optimize therapeutics used singly or in combinations to better block virus infection.

Another way to use antiviral is to give them prophylactically, especially to individuals at high risk of exposure. To better understand the early events in the acute stage of HIV infection stochastic models

were developed that follow the fate of individual infectious virions and infected cells^{91, 92}. A similar approach has been adopted for SARS-CoV-2 by Czuppon et al.⁹³ and used the model to predict what might occur when an individual taking antivirals prophylactically is exposed to different doses of infectious SARS-CoV-2. They studied the effects of four classes of antiviral: those that block viral entry or infection, those that block viral production from infected cells, e.g. remdesivir, those that enhance viral clearance such as a non-neutralizing antibody, and those such as an immunotoxin that can enhance infected cell death. Not surprisingly, they found that there is a critical drug efficacy needed to block establishment of infection that can depend on the drug's mechanism of action. Below this crucial efficacy, prophylaxis can still sometimes prevent establishment of infection especially with drugs that block viral entry or enhance viral clearance and can also flatten the viral kinetic curve possibly leading to less severe symptoms.

Overall, current modeling studies estimated that the critical drug efficacy to suppress viral infection in the setting of prophylaxis or treatment is roughly in the range between 85% and 95%^{44, 49, 93}.

Repurposing antivirals such as lopinavir/ritonavir, hydroxychloroquine and remdesivir is unlikely to achieve such high efficacy *in vivo*⁴⁴. Studies of human monoclonal antibodies, such as REGN-COV2 and bamlanivimab (LY-CoV555), showed that they are highly effective in suppressing viral replication, blocking infection and reducing viral load in both non-human primates and humans^{94, 95}.

They are likely to be highly efficacious *in vivo*, although formal model fitting to clinical data is needed for precise estimation of their antiviral efficacy. There are also mAbs in development that have Fc-effector functions and potentially could be used for treatment as these mAbs could in principle kill infected cells and mediate a vaccinal effect whereby presenting viral antigens to dendritic cells enhance T cell responses against the virus, e.g., Schafer et al.⁹⁶.

Linking viral load kinetics to infectiousness

Viral load in the URT is often used as a surrogate measure of infectiousness of a person. However, how these two quantities relate to each other is not clear. For example, both viral load and the logarithm of viral load are used as a measure of infectiousness for influenza infection⁹⁷. A quantitative framework to predict infectiousness of an individual from viral load measurements would be particularly useful for optimizing non-pharmaceutical interventions, such as test and trace strategies, as well as determining isolation duration after diagnosis. In a recent work, we addressed this question by comparing predictions from these two measures with epidemiological evidence. We found that the logarithm of the viral load better explains the observation that a large fraction of transmission occurs presymptomatically and that the serial interval is between 7-8 days without active intervention or self-isolation^{98, 99}. We then constructed a physiological model keeping track of each step of virus transmission process. A key aspect of this model is the assumption that the number of infectious viral particles reaching the recipient host given a contact is a saturating function of the viral load in the donor. A similar relationship was previously used for influenza and HIV transmission^{100, 101}, and was used by Goyal et al.¹⁰². This saturation effect explains why the logarithm of viral load is a better measure of infectiousness than the viral load⁴⁹.

Superspreading events were often reported for SARS-CoV-2 transmission¹⁰³. To understand these events, Goyal et al. generated an *in silico* population of infected individuals where their viral dynamics were simulated using parameters estimated from viral load data from hospitalized SARS-CoV-2 infected patients¹⁰². The transmission profiles for the individuals in the synthetic population were determined from their viral loads. Using their simulation, the authors show that variations in individual contact pattern (in addition to variations in individual viral load) play an important role in driving superspreading events¹⁰². It remains to be determined if other factors, such as heterogeneities in the level of infectious viruses⁵⁷, and mode of transmission, i.e. aerosol vs. droplet¹⁰⁴, also play important roles in driving these events.

Overall, these models serve as first steps towards predicting infectiousness from viral load data. Hopefully, as they develop, these models will prove useful in assessing the infectiousness of groups of infected individuals where viral load measurements are available and where epidemiological data are difficult to obtain or ascertain, such as asymptomatic individuals or children. Further improvement of the models, for example explicitly incorporating biological, physical and environmental factors during transmission^{104, 105}, will be needed to make more accurate and individual-level predictions.

Outstanding questions

Within less than a year, we have obtained extensive understanding of SARS-CoV-2 infection kinetics. As we summarized above, many viral dynamic models have been developed to estimate key parameters governing viral kinetics and determine how infectiousness depends on viral load. Models have also considered the effects of the immune responses and the impact of therapeutics. However, even though knowledge about SARS-CoV-2 is rapidly evolving, there are still many unknowns and questions that need to be addressed to help design both pharmaceutical and non-pharmaceutical intervention strategies.

Rate of exponential growth and the within host reproductive number, R_0

Despite many modeling efforts, there are still uncertainties in the rate of exponential expansion of the virus population during the early period of infection and thus in the within-host reproductive number R_0 . This prevents precise predictions of the drug efficacy needed to suppress the virus. The uncertainty arises from limitations in the data used for parameter estimation. First, for most of the datasets, the dates of initial infection are unknown. This makes estimation of the rate of exponential expansion unreliable. To address this issue, we recently used data from a study where infection dates were known through contact tracing⁴⁹. This greatly reduces uncertainty in the parameter estimation, and we found that the viral growth rate is negatively correlated with the incubation period⁴⁹. Second, in all datasets used for model inference so far, viral loads were measured after symptom onset, and the

viral load during the presymptomatic period, i.e. the phase of viral exponential growth, is unknown. In a recent study, frequent testing of both uninfected and infected individuals was performed, and this enabled viral load measurements during the presymptomatic phase of infection⁸⁷. This type of data will help to estimate the rate of exponential growth and the within-host reproductive number R_0 more accurately.

The relationship between SARS-CoV-2 viral load kinetics and disease severity

An important question is how differences in viral load may lead to different disease outcomes. Several clinical studies found that a high viral load at diagnosis or during later stages of infection is associated with more severe disease outcomes^{81, 82, 106}. This association is suggested to be a result of dysregulation of the immune responses^{64, 70, 107}. In severe cases, the antiviral response mediated by IFN is suppressed, resulting in a higher viral load, which in turn can lead to an exacerbated inflammatory response¹⁰⁸. Two recent studies highlighted the importance of the IFN response in preventing severe disease outcomes. One study shows that in 10% of severe COVID-19 cases, IFN was largely absent due to the presence of auto-antibodies targeting IFN¹⁰⁹, whereas another study¹¹⁰ showed that 3.5% of patients with life-threatening COVID-19 had inborn errors in genes associated with the IFN response. Therefore, modeling that aims to better understand the role of IFN responses^{68, 69} and the responses to proinflammatory cytokines will be useful for designing and understanding the impact of therapeutics to mitigate severe disease .

Other outstanding questions include how the size of the infection inoculum affects the interaction of the virus population with the immune system and disease outcome. Because of the nonlinear interactions among the virus, the innate and the adaptive immune system, modeling approaches are particularly well suited for addressing these questions⁷⁷.

Drug resistance

Mathematical models have been very successful and widely used to predict the risk of drug resistance in treating HIV, HCV and influenza infections^{9, 111, 112}. Many of these predictions have led to a profound impact on clinical practice. Currently, the antiviral remdesivir⁸⁹ is approved by the FDA, and many other antivirals and monoclonal antibodies^{94, 113, 114} may soon be approved for general use. Therefore, understanding and predicting drug resistance of SARS-CoV-2 will become important as we strive to identify the best strategies for treating patients.

One challenge to assessing the risk of resistance is to calculate the number of viruses produced during the course of infection¹¹² as mutation occurs during the replication of the viral RNA. Nonetheless, given the high viral load in many patients and the duration of viremia particularly in the LRT it is likely that all one-point mutations and some two-point mutations can be generated in an infected person¹¹². This suggests that resistant mutants can appear and rise to a high frequency quickly when an antiviral or an antibody with low genetic barrier to resistance (e.g. see ref. ¹¹³) is administered alone. Combinations therapies are preferred treatment strategy^{95, 113}. However, recent work suggests that a single amino-acid mutation can render the virus resistant to both antibodies in the REGN-COV2 cocktail¹¹⁵. Further clinical studies on drug resistant mutants and the cost of resistance are needed to precisely predict the risk of resistance and the genetic barriers needed to avoid selection of resistant mutants. These predictions can be further integrated into transmission models to evaluate how likely and how quickly drug resistance may spread in the population.

Conclusions

The interactions between viral and immune dynamics are highly complex and non-linear. The utility of mathematical models is to describe these non-linear interactions and allow for rigorous analysis and quantitative predictions. In this review we have strived to illustrate how this has worked for many viral infections and given us insights into viral pathogenesis and the effects of treatment. We believe these methods will also be beneficial in our attempts to tame the pandemic caused by SARS-CoV-2.

Acknowledgements

We thank Ruy M. Ribeiro for reading and commenting on the manuscript.

References:

1. Ho DD, *et al.* Rapid turnover of plasma virions and CD4 lymphocytes in HIV-1 infection. *Nature* **373** 123-126. (1995)
2. Wei X, *et al.* Viral dynamics in human immunodeficiency virus type 1 infection. *Nature* **373** 117-122. (1995)
3. Perelson AS, Neumann AU, Markowitz M, Leonard JM, Ho DD. HIV-1 dynamics in vivo: virion clearance rate, infected cell life-span, and viral generation time. *Science* **271** 1582-1586. (1996)
4. Perelson AS. Modelling viral and immune system dynamics. *Nat Rev Immunol* **2** 28-36. (2002)
5. Stafford MA, *et al.* Modeling plasma virus concentration during primary HIV infection. *J Theor Biol* **203** 285-301. (2000)
6. Perelson AS, Nelson PW. Mathematical analysis of HIV-1 dynamics in vivo. *SIAM Review* **41** 3-44. (1999)
7. Markowitz M, *et al.* A novel antiviral intervention results in more accurate assessment of human immunodeficiency virus type 1 replication dynamics and T-cell decay in vivo. *J Virol* **77** 5037-5038. (2003)
8. Ramratnam B, *et al.* Rapid production and clearance of HIV-1 and hepatitis C virus assessed by large volume plasma apheresis. *Lancet* **354** 1782-1785. (1999)

9. Perelson AS, Essunger P, Ho DD. Dynamics of HIV-1 and CD4+ lymphocytes in vivo. *AIDS* **11 Suppl A** S17-24. (1997)
10. Perelson AS, Ribeiro RM. Modeling the within-host dynamics of HIV infection. *BMC biology* **11** 96. (2013)
11. Perelson AS, *et al.* Decay characteristics of HIV-1-infected compartments during combination therapy. *Nature* **387** 188-191. (1997)
12. Louie M, *et al.* Determining the relative efficacy of highly active antiretroviral therapy. *J Infect Dis* **187** 896-900. (2003)
13. Shudo E, Ribeiro RM, Talal AH, Perelson AS. A hepatitis C viral kinetic model that allows for time-varying drug effectiveness. *Antivir Ther* **13** 919-926. (2008)
14. Wu H, *et al.* Pharmacodynamics of antiretroviral agents in HIV-1 infected patients: using viral dynamic models that incorporate drug susceptibility and adherence. *J Pharmacokinet Pharmacodyn* **33** 399-419. (2006)
15. Wu H, *et al.* Modeling long-term HIV dynamics and antiretroviral response: effects of drug potency, pharmacokinetics, adherence, and drug resistance. *J Acquir Immune Defic Syndr* **39** 272-283. (2005)
16. Talal AH, *et al.* Pharmacodynamics of PEG-IFN alpha differentiate HIV/HCV coinfecting sustained virological responders from nonresponders. *Hepatology* **43** 943-953. (2006)

- Accepted Article
17. Guedj J, *et al.* Modeling viral kinetics and treatment outcome during alisporivir interferon-free treatment in hepatitis C virus genotype 2 and 3 patients. *Hepatology* **59** 1706-1714. (2014)
 18. Canini L, *et al.* A pharmacokinetic/viral kinetic model to evaluate the treatment effectiveness of danoprevir against chronic HCV. *Antivir Ther* **20** 469-477. (2015)
 19. Herz AV, Bonhoeffer S, Anderson RM, May RM, Nowak MA. Viral dynamics in vivo: limitations on estimates of intracellular delay and virus decay. *Proc Natl Acad Sci U S A* **93** 7247-7251. (1996)
 20. Mittler JE, Sulzer B, Neumann AU, Perelson AS. Influence of delayed viral production on viral dynamics in HIV-1 infected patients. *Math Biosci* **152** 143-163. (1998)
 21. Mittler JE, Markowitz M, Ho DD, Perelson AS. Improved estimates for HIV-1 clearance rate and intracellular delay. *AIDS* **13** 1415-1417. (1999)
 22. Holder BP, Beauchemin CA. Exploring the effect of biological delays in kinetic models of influenza within a host or cell culture. *BMC Public Health* **11 Suppl 1** S10. (2011)
 23. Beauchemin CA, Miura T, Iwami S. Duration of SHIV production by infected cells is not exponentially distributed: Implications for estimates of infection parameters and antiviral efficacy. *Sci Rep* **7** 42765. (2017)
 24. Baccam P, Beauchemin C, Macken CA, Hayden FG, Perelson AS. Kinetics of influenza A virus infection in humans. *J Virol* **80** 7590-7599. (2006)

25. Best K, *et al.* Zika plasma viral dynamics in nonhuman primates provides insights into early infection and antiviral strategies. *Proc Natl Acad Sci U S A* **114** 8847-8852. (2017)
26. Best K, Perelson AS. Mathematical modeling of within-host Zika virus dynamics. *Immunol Rev* **285** 81-96. (2018)
27. Nelson PW, Gilchrist MA, Coombs D, Hyman JM, Perelson AS. An age-structured model of hiv infection that allows for variations in the production rate of viral particles and the death rate of productively infected cells. *Math Biosci Eng* **1** 267-288. (2004)
28. Finzi D, *et al.* Latent infection of CD4+ T cells provides a mechanism for lifelong persistence of HIV-1, even in patients on effective combination therapy. *Nat Med* **5** 512-517. (1999)
29. Sengupta S, Siliciano RF. Targeting the Latent Reservoir for HIV-1. *Immunity* **48** 872-895. (2018)
30. Neumann AU, *et al.* Hepatitis C viral dynamics in vivo and the antiviral efficacy of interferon-alpha therapy. *Science* **282** 103-107. (1998)
31. Guedj J, *et al.* Modeling shows that the NS5A inhibitor daclatasvir has two modes of action and yields a shorter estimate of the hepatitis C virus half-life. *Proc Natl Acad Sci U S A* **110** 3991-3996. (2013)
32. Ke R, *et al.* Modelling clinical data shows active tissue concentration of daclatasvir is 10-fold lower than its plasma concentration. *J Antimicrob Chemother* **69** 724-727. (2014)
33. Hinrichsen H, *et al.* Short-term antiviral efficacy of BILN 2061, a hepatitis C virus serine protease inhibitor, in hepatitis C genotype 1 patients. *Gastroenterology* **127** 1347-1355. (2004)

- Accepted Article
34. Herrmann E, *et al.* Viral kinetics in patients with chronic hepatitis C treated with the serine protease inhibitor BILN 2061. *Antivir Ther* **11** 371-376. (2006)
 35. Snoeck E, *et al.* A comprehensive hepatitis C viral kinetic model explaining cure. *Clin Pharmacol Ther* **87** 706-713. (2010)
 36. Kitagawa K, Nakaoka S, Asai Y, Watashi K, Iwami S. A PDE multiscale model of hepatitis C virus infection can be transformed to a system of ODEs. *J Theor Biol* **448** 80-85. (2018)
 37. McGivern DR, *et al.* Protease Inhibitors Block Multiple Functions of the NS3/4A Protease-Helicase during the Hepatitis C Virus Life Cycle. *J Virol* **89** 5362-5370. (2015)
 38. McGivern DR, *et al.* Kinetic analyses reveal potent and early blockade of hepatitis C virus assembly by NS5A inhibitors. *Gastroenterology* **147** 453-462 e457. (2014)
 39. Goncalves A, *et al.* What drives the dynamics of HBV RNA during treatment? *J Viral Hepat* <https://doi.org/10.1111/jvh.13425>. (2020)
 40. Pawelek KA, *et al.* Modeling within-host dynamics of influenza virus infection including immune responses. *PLoS Comput Biol* **8** e1002588. (2012)
 41. Banerjee S, Guedj J, Ribeiro RM, Moses M, Perelson AS. Estimating biologically relevant parameters under uncertainty for experimental within-host murine West Nile virus infection. *J R Soc Interface* **13**. (2016)

- Accepted Article
42. Wethington D, *et al.* Mathematical modelling identifies the role of adaptive immunity as a key controller of respiratory syncytial virus in cotton rats. *J R Soc Interface* **16** 20190389. (2019)
 43. Dobrovolny HM. Quantifying the effect of remdesivir in rhesus macaques infected with SARS-CoV-2. *Virology* **550** 61-69. (2020)
 44. Gonçalves A, *et al.* Timing of antiviral treatment initiation is critical to reduce SARS-CoV-2 viral load. *CPT: Pharmacometrics & Systems Pharmacology* **9** 509-514. (2020)
 45. Goyal A, Cardozo-Ojeda EF, Schiffer JT. Potency and timing of antiviral therapy as determinants of duration of SARS-CoV-2 shedding and intensity of inflammatory response. *Sci Adv* **6** eabc7112. (2020)
 46. Goyal A, Duke ER, Cardozo-Ojeda EF, Schiffer JT. Mathematical modeling explains differential SARS CoV-2 kinetics in lung and nasal passages in remdesivir treated rhesus macaques. *bioRxiv* <https://doi.org/10.1101/2020.1106.1121.163550>. (2020)
 47. Hernandez-Vargas EA, Velasco-Hernandez JX. In-host Mathematical Modelling of COVID-19 in Humans. *Annu Rev Control* **50** 448-456. (2020)
 48. Iwanami S, *et al.* Rethinking antiviral effects for COVID-19 in clinical studies: early initiation is key to successful treatment. *medRxiv* doi: 10.1101/2020.1105.1130.20118067. (2020)
 49. Ke R, Zitzmann C, Ribeiro RM, Perelson AS. Kinetics of SARS-CoV-2 infection in the human upper and lower respiratory tracts and their relationship with infectiousness. *medRxiv* <https://doi.org/10.1101/2020.1109.1125.20201772>. (2020)

50. Kim KS, *et al.* Modelling SARS-CoV-2 Dynamics: Implications for Therapy. *medRxiv* <https://doi.org/10.1101/2020.1103.1123.20040493>. (2020)
51. Wang S, *et al.* Modeling the viral dynamics of SARS-CoV-2 infection. *Math Biosci* **328** 108438. (2020)
52. Tarek M, Savarino A. Pharmacokinetic Basis of the Hydroxychloroquine Response in COVID-19: Implications for Therapy and Prevention. *Eur J Drug Metab Pharmacokinet* **45** 715-723. (2020)
53. Goncalves A, *et al.* Viral dynamic modeling of SARS-CoV-2 in non-human primates. *PREPRINT (Version 1) available at Research Square [available at: <https://www.researchsquare.com/article/rs-50301/v1>]*. (2020)
54. Smith AM, Perelson AS. Influenza A virus infection kinetics: quantitative data and models. *Wiley Interdiscip Rev Syst Biol Med* **3** 429-445. (2011)
55. Smith AM, Ribeiro RM. Modeling the viral dynamics of influenza A virus infection. *Crit Rev Immunol* **30** 291-298. (2010)
56. To KK, *et al.* Temporal profiles of viral load in posterior oropharyngeal saliva samples and serum antibody responses during infection by SARS-CoV-2: an observational cohort study. *Lancet Infect Dis* **20** 565-574. (2020)
57. Wolfel R, *et al.* Virological assessment of hospitalized patients with COVID-2019. *Nature* **581** 465-469. (2020)

58. Williamson BN, *et al.* Clinical benefit of remdesivir in rhesus macaques infected with SARS-CoV-2. *Nature* **585** 273-276. (2020)
59. Muus C, *et al.* Integrated analyses of single-cell atlases reveal age, gender, and smoking status associations with cell type-specific expression of mediators of SARS-CoV-2 viral entry and highlights inflammatory programs in putative target cells. *bioRxiv* DOI: 10.1101/2020.1104.1119.049254. (2020)
60. Sungnak W, *et al.* SARS-CoV-2 entry factors are highly expressed in nasal epithelial cells together with innate immune genes. *Nat Med* **26** 681-687. (2020)
61. Hou YJ, *et al.* SARS-CoV-2 reverse genetics reveals a variable infection gradient in the respiratory tract. *Cell* **182** 429-446 e414. (2020)
62. Ogando NS, *et al.* SARS-coronavirus-2 replication in Vero E6 cells: replication kinetics, rapid adaptation and cytopathology. *J Gen Virol* **101** 925-940. (2020)
63. Tay MZ, Poh CM, Renia L, MacAry PA, Ng LFP. The trinity of COVID-19: immunity, inflammation and intervention. *Nat Rev Immunol* **20** 363-374. (2020)
64. Blanco-Melo D, *et al.* Imbalanced host response to SARS-CoV-2 drives development of COVID-19. *Cell* **181** 1036-1045 e1039. (2020)
65. Holte SE, Melvin AJ, Mullins JI, Tobin NH, Frenkel LM. Density-dependent decay in HIV-1 dynamics. *J Acquir Immune Defic Syndr* **41** 266-276. (2006)

66. Smith AP, Moquin DJ, Bernhauerova V, Smith AM. Influenza Virus Infection Model With Density Dependence Supports Biphasic Viral Decay. *Front Microbiol* **9** 1554. (2018)
67. Gallagher ME, Brooke CB, Ke R, Koelle K. Causes and Consequences of Spatial Within-Host Viral Spread. *Viruses* **10** 627. (2018)
68. Huang Y, Dai H, Ke R. Principles of Effective and Robust Innate Immune Response to Viral Infections: A Multiplex Network Analysis. *Front Immunol* **10** 1736. (2019)
69. Lavigne GM, Russell H, Sherry B, Ke R. Autocrine and paracrine interferon signaling as 'ring vaccination' and 'contact tracing' strategies to suppress virus infection in a host. *medRxiv* <https://doi.org/10.1101/2020.1112.1109.20246777>. (2020)
70. Lucas C, *et al.* Longitudinal analyses reveal immunological misfiring in severe COVID-19. *Nature* **584** 463-469. (2020)
71. Channappanavar R, *et al.* IFN-I response timing relative to virus replication determines MERS coronavirus infection outcomes. *J Clin Invest* **129** 3625-3639. (2019)
72. Best K, Barouch DH, Gudej J, Ribeiro RM, Perelson AS. Zika virus dynamics: Effects of inoculum dose, the innate immune response and viral interference. *PLoS Comput Biol.* (in press)
73. Padmanabhan P, Garaigorta U, Dixit NM. Emergent properties of the interferon-signalling network may underlie the success of hepatitis C treatment. *Nat Commun* **5** 3872. (2014)

74. Weiskopf D, *et al.* Phenotype and kinetics of SARS-CoV-2-specific T cells in COVID-19 patients with acute respiratory distress syndrome. *Sci Immunol* **5** eabd2071. (2020)
75. Braun J, *et al.* SARS-CoV-2-reactive T cells in healthy donors and patients with COVID-19. *Nature* **587** 270-274. (2020)
76. De Boer RJ, Homann D, Perelson AS. Different dynamics of CD4+ and CD8+ T cell responses during and after acute lymphocytic choriomeningitis virus infection. *J Immunol* **171** 3928-3935. (2003)
77. Baral S, Antia R, Dixit NM. A dynamical motif comprising the interactions between antigens and CD8 T cells may underlie the outcomes of viral infections. *Proc Natl Acad Sci U S A* **116** 17393-17398. (2019)
78. Getz M, *et al.* Rapid community-driven development of a SARS-CoV-2 tissue simulator. *bioRxiv* <https://doi.org/10.1101/2020.1104.1102.019075>. (2020)
79. Sego TJ, *et al.* A modular framework for multiscale, multicellular, spatiotemporal modeling of acute primary viral infection and immune response in epithelial tissues and its application to drug therapy timing and effectiveness. *bioRxiv* doi: 10.1101/2020.1104.1127.064139. (2020)
80. Voutouri C, *et al.* In silico dynamics of COVID-19 phenotypes for optimizing clinical management. *Proc Natl Acad Sci USA* **118** e2021642118 (2021)
81. Fajnzylber J, *et al.* SARS-CoV-2 viral load is associated with increased disease severity and mortality. *Nat Commun* **11** 5493. (2020)
82. Zheng S, *et al.* Viral load dynamics and disease severity in patients infected with SARS-CoV-2 in Zhejiang province, China, January-March 2020: retrospective cohort study. *BMJ* **369** m1443. (2020)

83. Barkauskas CE, *et al.* Type 2 alveolar cells are stem cells in adult lung. *J Clin Invest* **123** 3025-3036. (2013)
84. Dahari H, Lo A, Ribeiro RM, Perelson AS. Modeling hepatitis C virus dynamics: liver regeneration and critical drug efficacy. *J Theor Biol* **247** 371-381. (2007)
85. Goyal A, Ribeiro RM, Perelson AS. The Role of Infected Cell Proliferation in the Clearance of Acute HBV Infection in Humans. *Viruses* **9** 350. (2017)
86. Perelson AS, Kirschner DE, De Boer R. Dynamics of HIV infection of CD4+ T cells. *Math Biosci* **114** 81-125. (1993)
87. Kissler SM, *et al.* Viral dynamics of SARS-CoV-2 infection and the predictive value of repeat testing. *medRxiv* <https://doi.org/10.1101/2020.1110.1121.20217042>. (2020)
88. Sakurai A, *et al.* Natural history of asymptomatic SARS-CoV-2 infection. *N Engl J Med* **383** 885-886. (2020)
89. Beigel JH, *et al.* Remdesivir for the Treatment of Covid-19 - Final Report. *N Engl J Med* **383** 1813-1826. (2020)
90. Wang Y, *et al.* Remdesivir in adults with severe COVID-19: a randomised, double-blind, placebo-controlled, multicentre trial. *Lancet* **395** 1569-1578. (2020)

91. Pearson JE, Krapivsky P, Perelson AS. Stochastic theory of early viral infection: continuous versus burst production of virions. *PLoS Comput Biol* **7** e1001058. (2011)
92. Noecker C, *et al.* Simple mathematical models do not accurately predict early SIV dynamics. *Viruses* **7** 1189-1217. (2015)
93. Czuppon P, *et al.* Success of prophylactic antiviral therapy for SARS-CoV-2: predicted critical efficacies and impact of different drug-specific mechanisms of action. *medRxiv* <https://doi.org/10.1101/2020.1105.1107.20092965>. (2020)
94. Chen P, *et al.* SARS-CoV-2 Neutralizing Antibody LY-CoV555 in Outpatients with Covid-19. *N Engl J Med* DOI: 10.1056/NEJMoa2029849. (2020)
95. Baum A, *et al.* REGN-COV2 antibodies prevent and treat SARS-CoV-2 infection in rhesus macaques and hamsters. *Science* **370** 1110-1115. (2020)
96. Schafer A, *et al.* Antibody potency, effector function, and combinations in protection and therapy for SARS-CoV-2 infection in vivo. *J Exp Med* **218** e20201993. (2021)
97. Handel A, Rohani P. Crossing the scale from within-host infection dynamics to between-host transmission fitness: a discussion of current assumptions and knowledge. *Philos Trans R Soc Lond B Biol Sci* **370** 20140302. (2015)
98. Ali ST, *et al.* Serial interval of SARS-CoV-2 was shortened over time by nonpharmaceutical interventions. *Science* **369** 1106-1109. (2020)

- Accepted Article
99. He X, *et al.* Temporal dynamics in viral shedding and transmissibility of COVID-19. *Nat Med* **26** 672-675. (2020)
 100. Fraser C, Hollingsworth TD, Chapman R, de Wolf F, Hanage WP. Variation in HIV-1 set-point viral load: epidemiological analysis and an evolutionary hypothesis. *Proc Natl Acad Sci U S A* **104** 17441-17446. (2007)
 101. Handel A, Longini IM, Jr., Antia R. Neuraminidase inhibitor resistance in influenza: assessing the danger of its generation and spread. *PLoS Comput Biol* **3** e240. (2007)
 102. Goyal A, Reeves DB, Cardozo-Ojeda EF, Schiffer JT, Mayer BT. Wrong person, place and time: viral load and contact network structure predict SARS-CoV-2 transmission and super-spreading events. *medRxiv* <https://doi.org/10.1101/2020.1108.1107.20169920>. (2020)
 103. Lau MSY, *et al.* Characterizing superspreading events and age-specific infectiousness of SARS-CoV-2 transmission in Georgia, USA. *Proc Natl Acad Sci U S A* **117** 22430-22435. (2020)
 104. Klompas M, Baker MA, Rhee C. Airborne Transmission of SARS-CoV-2: Theoretical Considerations and Available Evidence. *JAMA* **324** 441-442. (2020)
 105. Morris DH, *et al.* The effect of temperature and humidity on the stability of SARS-CoV-2 and other enveloped viruses. *bioRxiv* <https://doi.org/10.1101/2020.1110.1116.341883>. (2020)
 106. Pujadas E, *et al.* SARS-CoV-2 viral load predicts COVID-19 mortality. *Lancet Respir Med* **8** e70. (2020)

- Accepted Article
107. Rydzynski Moderbacher C, *et al.* Antigen-specific adaptive immunity to SARS-CoV-2 in acute COVID-19 and associations with age and disease severity. *Cell* **183** 1-17. (2020)
 108. Hadjadj J, *et al.* Impaired type I interferon activity and exacerbated inflammatory responses in severe Covid-19 patients. *Science* **369** 718-724. (2020)
 109. Bastard P, *et al.* Autoantibodies against type I IFNs in patients with life-threatening COVID-19. *Science* **370** eabd4585. (2020)
 110. Zhang Q, *et al.* Inborn errors of type I IFN immunity in patients with life-threatening COVID-19. *Science* **370** eabd4570. (2020)
 111. Rong L, Dahari H, Ribeiro RM, Perelson AS. Rapid emergence of protease inhibitor resistance in hepatitis C virus. *Sci Transl Med* **2** 30ra32. (2010)
 112. Perelson AS, Rong L, Hayden FG. Combination antiviral therapy for influenza: predictions from modeling of human infections. *J Infect Dis* **205** 1642-1645. (2012)
 113. Baum A, *et al.* Antibody cocktail to SARS-CoV-2 spike protein prevents rapid mutational escape seen with individual antibodies. *Science* **369** 1014-1018. (2020)
 114. Hansen J, *et al.* Studies in humanized mice and convalescent humans yield a SARS-CoV-2 antibody cocktail. *Science* **369** 1010-1014. (2020)
 115. Starr TN, *et al.* Prospective mapping of viral mutations that escape antibodies used to treat COVID-19. *bioRxiv* doi: 10.1101/2020.1111.1130.405472. (2020)

Figure Legends.

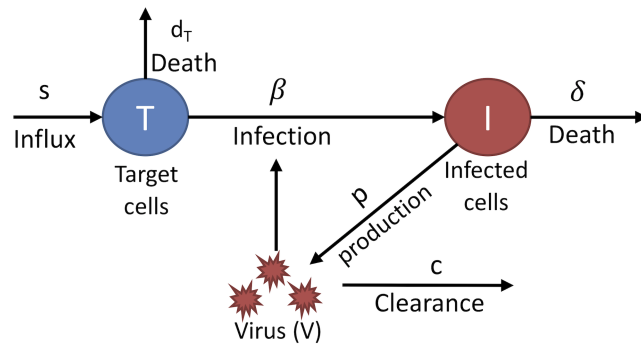
Fig. 1. The basic model of viral infection. Target cells, T , which are cells susceptible to infection, are infected by virus, V , with rate constant β . Target cells are assumed to be made by a source at rate s and to die at per capita rate d_T . Infected cells, I , produce virus as rate p per cell and die at rate δ per cell. Free virus particles, V , are cleared at per capita rate c .

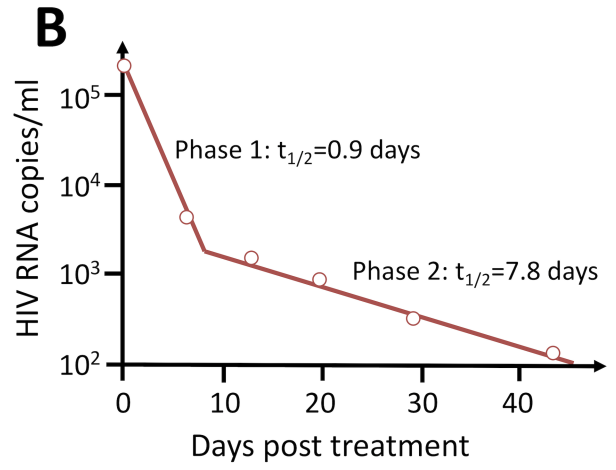
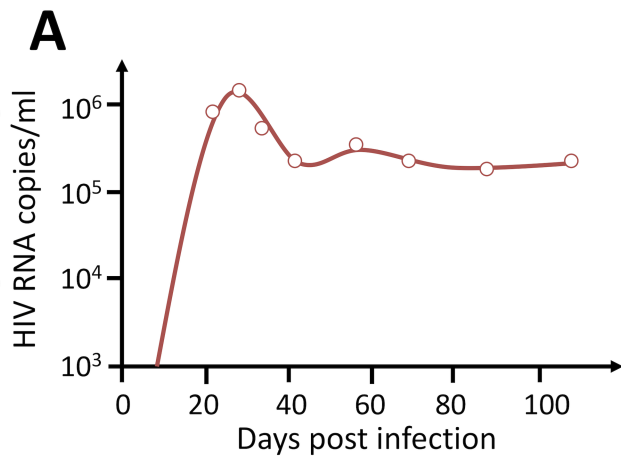
Fig. 2. Modeling HIV infection and treatment. (A) The basic model can fit data (open circles) taken from individuals newly infected with HIV-1. The model solution (solid line) illustrates that virus initially grows exponentially, reaches a peak then falls and ultimately approaches a steady-state called the viral set-point. See Ref ⁵ for details. (B) Biphasic decline of HIV-1 RNA after potent antiretroviral therapy is initiated. The basic model augmented with a population of long-lived infected cells (solid line) fits data taken from chronically infected HIV patients placed on combination antiretroviral therapy. The slopes of the first phase and second phase declines are mainly determined by the loss rate of short-lived and long-lived infected cells, respectively. See Ref ¹¹ for details.

Fig. 3. Dynamics of HCV RNA decline after therapy initiation. (A) Fit of Eq. (9) (solid line) to data from an HCV chronically infected patient treated with IFN given daily. After a very brief delay the viral load falls rapidly by about $1.5 \log_{10}$ and appears to be approaching a steady state. (B) On a longer-time scale the viral load continues to fall. The solid line shows the best-fit solution of Eqs, (1a), (1b) and (8) to the data. As discussed in Ref ³⁰, the slope of the first phase decline mainly reflects the rate of viral clearance, c , whereas the slope of the second phase decline mainly reflects the rate of loss of infected cells, δ . The magnitude of the first phase decline determines the efficacy of the drug. When a more potent DAA, such as the NS5A inhibitor daclatasvir is used the first phase decline can be 3 logs, implying a drug effectiveness of 99.9%. See ref ³¹ for details.

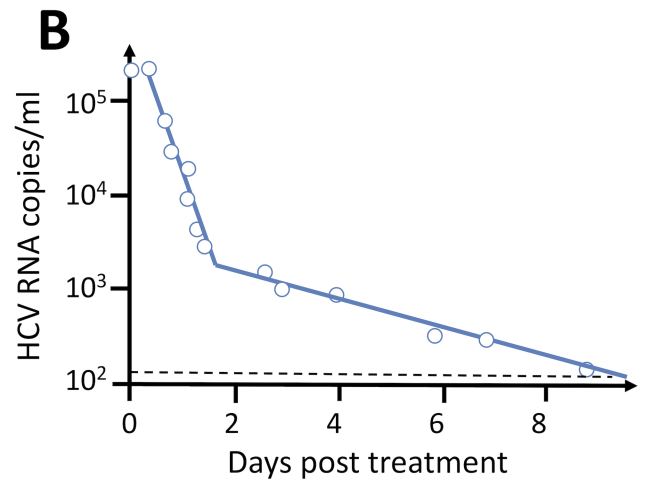
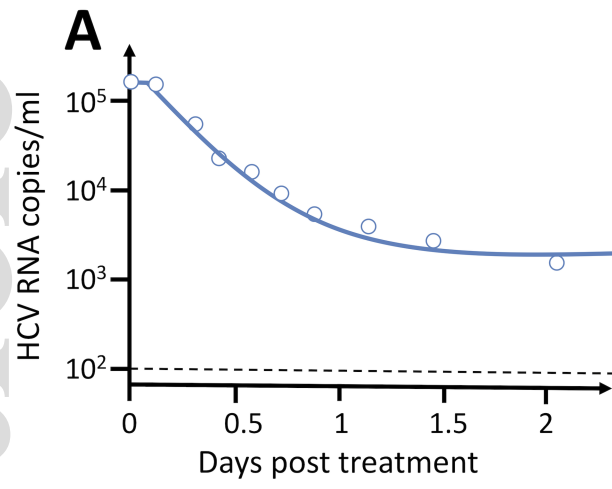
Fig. 4. Illustration of the dynamics of SARS-CoV-2 infection in the upper respiratory tract (URT; solid red line) and the lower respiratory tract (LRT; solid blue line). The incubation period lasts for approximately 4-6 days (5 day is shown in the figure). The virus population reaches peak viral load at or a couple of days post symptom onset. Individuals become infectious at or a few days before symptom onset. The viral load declines rapidly after peak viremia in the URT, whereas

the viral load in the LRT is maintained at intermediate-to-high levels for several weeks. Dotted and dashed lines denote predicted viral load dynamics when individuals are treated with an effective antiviral (e.g. with 95% efficacy) at symptom onset (dotted lines), or 8 days post symptom onset (dashed lines). Viral load curves are drawn based on the data in Refs. ^{57, 82} and parameter estimates in Ref. ⁴⁹.

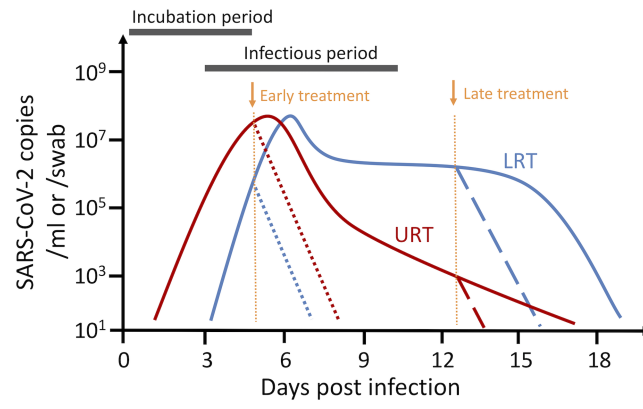




cpt_2160_f2.tif



cpt_2160_f3.tif



cpt_2160_f4.tif